This is a preprint that has not yet undergone peer-review.
Manuscript submitted to *Earth Surface Processes and Landforms*.

A systematic approach and software for the analysis of point patterns on river networks

Wolfgang Schwanghart[1*], Christian Molkenthin[2], Dirk Scherler[3,4]

1 Institute of Environmental Science and Geography, University of Potsdam, 14476 Potsdam-Golm, Germany

2 Institute of Mathematics, University of Potsdam, 14476 Potsdam-Golm, Germany

3 German Research Centre for Geosciences (GFZ), Earth Surface Geochemistry, 14473 Potsdam, Germany

4 Institute of Geological Sciences, Freie Universität Berlin, 12249 Berlin, Germany

* Corresponding author: w.schwanghart@geo.uni-potsdam.de

Keywords: Point pattern analysis, point processes, fluvial geomorphology, knickpoints, beaver dams

Abstract

Many geomorphic phenomena such as bank failures, landslide dams, riffle-pool sequences and knickpoints can be modelled as spatial point processes. However, as the locations of these phenomena are constrained to lie on or alongside rivers, their analysis must account for the geometry and topology of river networks. Here, we introduce a new numeric class in TopoToolbox called Point Pattern on Stream networks (PPS), which supports exploratory analysis, statistical modelling, simulation and visualization of point processes. We present two case studies that aim at inferring processes and factors that control the spatial density of geomorphic phenomena along river networks: the analysis of knickpoints in river profiles, and modelling spatial locations of beaver dams based on topographic metrics. The case studies rely on exploratory analysis and statistical inference using inhomogeneous Poisson point processes. Thereby, statistical and probabilistic procedures implemented in PPS provide a systematic approach for treating of uncertainties. PPS provides a consistent numeric framework for modelling point processes on river networks with a wide range of applications in fluvial geomorphology, but also other disciplines such as ecology.

Introduction

Many geomorphic phenomena along rivers can be represented as spatial point processes. For example, bank failures (Fonstad and Marcus, 2003; Liang et al., 2015), landslide dams (Fan et al., 2020; Korup, 2006; Tacconi Stefanelli et al., 2015), riffle-pool sequences (Golly et al., 2019), wood jams (Scott et al., 2019; Wohl, 2013), and knickpoints (Berlin and Anderson, 2007; Gailleton et al., 2019; Phillips and Lutz, 2008; Schwanghart and Scherler, 2020) are phenomena that occur at specific locations along rivers and that – at particular spatial scales of analysis – can be represented as point features. Many questions about these processes are inherently linked to their spatial arrangement. For example: Do these phenomena occur randomly in space, or are there mechanisms that cause these phenomena to cluster spatially? Are there interactions between these phenomena that generate some characteristic spacing between them or do additional factors exist that promote their spatial density? A spatial point process is a stochastic mechanism that generates patterns of points in space. The analysis of point patterns – a major subject within the field of spatial statistics – is concerned with understanding and modelling the stochastic and deterministic mechanisms that generate the patterns (Baddeley et al., 2015). While point pattern analysis has pervaded many geoscientific disciplines, applications in geomorphology are relatively rare (Bishop, 2007b, 2007a; Clark et al., 2018; Kandakji et al., 2020; Kraft et al., 2011; Lombardo et al., 2018, 2019; Oeppen and Ongley, 1975; Sochan et al., 2019; Tarboton et al., 1989).

The aim of this study is to explore the opportunities that the analysis of spatial point patterns offers in geomorphology. In particular, we are interested in point patterns that occur along river networks. The network-led spatial configuration makes this kind of analysis challenging. Statistical techniques designed for point patterns in two-dimensional space are usually based on the Euclidean distance between points which can be very different from distances along networks (Ang et al., 2012; Okabe et al., 2009). While methodological developments in geostatistics have established a mature set of tools to tackle interpolation along stream networks (Cressie et al., 2006; Ganio et al., 2005; Skoien et al., 2006; Ver Hoef et al., 2006), point pattern analysis on networks is a relatively young and active field of research (Baddeley et al., 2015; Okabe and Sugihara, 2012).

Here, we present an extension to the MATLAB-based terrain analysis software TopoToolbox (Schwanghart and Kuhn, 2010; Schwanghart and Scherler, 2014) called PPS (Point Pattern on Stream networks), which implements the statistical principles and techniques of point pattern analysis on linear networks. PPS complements other tools for point pattern analysis. The R-package spatstat is among the most comprehensive software packages that also handles point patterns on networks (Baddeley et al., 2015) and has strongly influenced the design of PPS. In addition, SANET (Okabe et al., 2018) is a toolbox for ArcGIS for analyzing events that occur on networks or alongside networks. Incorporating PPS in TopoToolbox offers seamless workflows including data import, analysis, modelling and visualization in the MATLAB programming environment. The ease of working in one computational programming environment and the availability of computational tools for working with river network data was a major motivation to develop PPS alongside TopoToolbox.

In the following text, we provide a brief summary of the theory, computational methods, and implementation of PPS. We furthermore present two applications in which point pattern analysis serves as an approach to investigating and modelling the occurrence of geomorphic forms and processes along river networks.

Point processes on networks

Spatial analysis of point patterns is predicated on the concept of first and second order effects or variations. First order variations arise from spatial trends or other covariates that control the spatial density of points. For example, the spatial density of bank collapses along a river is a function of the type of rocks or sediments, but may additionally be controlled by spatial trends in water level fluctuations, river gradient and planform geometry (Fonstad and Marcus, 2003; Liang et al., 2015). Bank collapses can also impact the occurrence of other events of bank failures. Once a bank has failed it may change patterns of river flow and/or make adjacent banks susceptible to failure due to debuttressing. Close to an existing bank failure we might thus expect even more bank failures. In this case, we hypothesize a second order effect due to direct physical interactions that cause bank collapses to be more frequent close to other failures. Another example for a second order variation is the effect of seed dispersal on the spatial density of plants, but we may also think of processes that inhibit small distances between adjacent points such as the competition for nutrients, light and water. In fluvial geomorphology, riffle-pool and step-pool sequences are phenomena that exhibit regular distances (Golly et al., 2019; Knighton, 1998; Tarboton et al., 1989). A major goal of point pattern analysis pertains to the analysis and modelling of first and second order variations from point data (Baddeley et al., 2015). Although this might appear straightforward at first glance, separating the two effects from each other is often challenging.

Commonly, spatial point processes are analyzed in two or three spatial dimensions and time. Frequently, however, the events (entities, points, locations) occur on or alongside networks. Car accidents, for example, are events on a road network whereas supermarkets are locations alongside the road network. Whether on or alongside, the coordinates of these points are constrained by a spatial network (network-constrained events or, in short, network events (Okabe and Sugihara, 2012)). Paths between points follow the network's edges and thus distances rarely follow direct Euclidean distances. Instead, standard practice is to measure distances in networks by the length of the shortest path, least-cost or resistance distances (Rakshit et al., 2017). To this end, many existing methods in point pattern analysis rely on the Euclidean distance which may be inappropriate or fallacious if applied to network events (Okabe and Sugihara, 2012; Rakshit et al., 2017) (Figure 1). It may seem straightforward that distances in river networks ought to be calculated in metric units from the outlet or channelheads, but we may also weight these distances by stream flow (Ver Hoef et al., 2006) or elevation (Foltête et al., 2008), or use metrics such as χ-transformed distance (Harkins et al., 2007; Perron and Royden, 2013) which are increasingly used in the analysis of river profiles and network topology. The choice of distance metric depends on the application and should be guided by additional information (Rakshit et al., 2017). Hence, not all network-constrained points must be analyzed using network-derived distances. In an analysis of the spatial patterns of river junctions, for example, Oeppen and Ongley (1975) relied on the planar Euclidean distance.

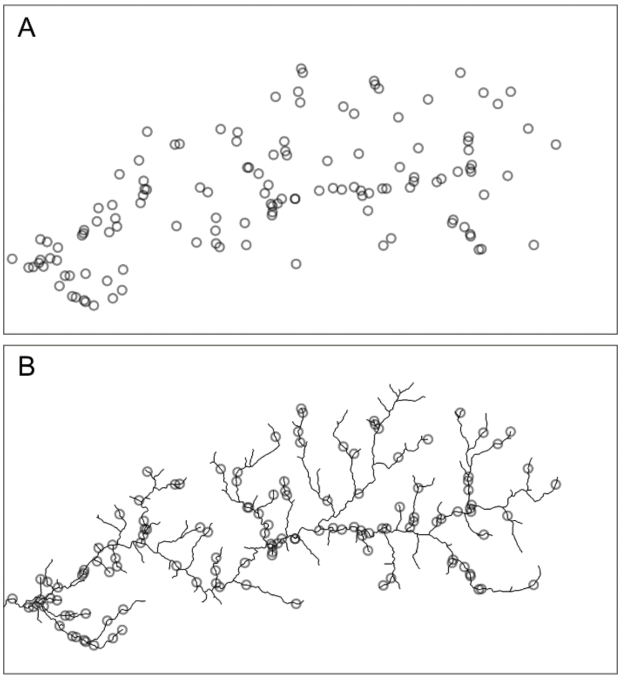

Figure 1: Spatial point processes clearly lack a completely random pattern (A) if we ignore that their locations are constrained by a network. If we take this constraint into account (B), it is more difficult to decide if the observed point pattern is completely random or not.

TopoToolbox as the basis for PPS

PPS is based on TopoToolbox, a MATLAB software for topographic analysis (Schwanghart and Scherler, 2014). TopoToolbox pursues an object-oriented programming approach that simplifies programming tasks which involve gridded digital elevation models (DEMs) and topographic derivatives (Figure 2). A DEM is stored as an object of the class GRIDobj which includes the matrix of elevation values and information on extent, resolution, and coordinate reference system. Flow directions are derived from DEMs and are stored as an instance of the class FLOWobj. Using topological sorting of the flow network (Braun and Willett, 2013; Hergarten and Neugebauer, 2001), this computational object enables the derivation of drainage basins or computations such as flow accumulation (Schwanghart and Scherler, 2014). Moreover, FLOWobj is the basis for the delineation of stream networks which are stored as an object of the class STREAMobj. Any computation with stream networks adopts highly efficient algorithms from graph theory (Heckmann et al., 2015). PPS takes advantage of the algorithms that are readily available in TopoToolbox and extends their capabilities to numerous new applications that enable the analysis of point patterns on stream networks (Figure 2).

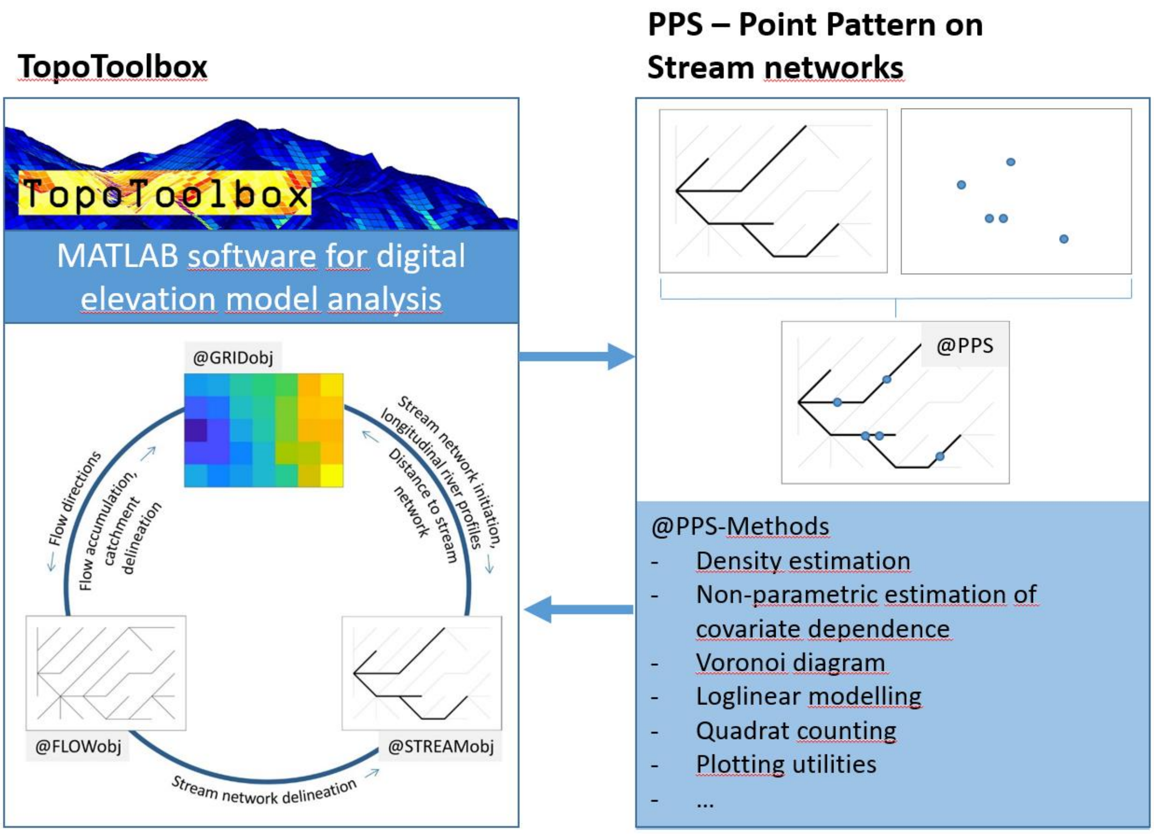

Figure 2: Numerical classes in TopoToolbox and the new PPS class.

Numeric implementation and methods of PPS

Computational representations of networks can rely on either vector or raster representations (Okabe and Sugihara, 2012). Being built on the STREAMobj class, PPS uses a hybrid approach. An object of class STREAMobj is derived from a DEM. Thus, the nodes of the PPS stream network refer to cell centers of the DEM. The topology of the network is determined by edges that link the cell centers in cardinal and diagonal directions (8-connectivity). Each node in the network can have attribute values which we refer to as node-attribute list. An instance of PPS is created by combining a stream network with a point dataset represented by a set of coordinates. If the points are not located on the stream network, they are snapped to the nearest nodes of the stream network, and their distance to the stream can be an attribute of the points. Formally, PPS thus adopts a fine-pixel approximation of a point pattern (Baddeley et al., 2015).

Table 1: Overview on PPS functions.

Function	Description
Creating an instance of PPS	

PPS	Constructor function that creates an instance of class PPS from a stream network (STREAMobj) and a set of points. Alternatively, the function can generate randomly distributed points on stream networks, or calculate intersections with a network of lines.
Explorative analysis	
density	Kernel density estimator on stream networks
ecdf	Empirical cumulative density function
intensity	Intensity (points per unit distance)
histogram	Histogram of point pattern on stream network
rhohat	Nonparametric estimation of covariate dependence
cluster	Hierarchical spatial clustering of points
Inference and simulation	
fitloglinear	Fitting a loglinear intensity model
bayesloglinear	Bayesian analysis of a loglinear intensity model
quadratcount	Quadrat counting
random	Simulation of points using a loglinear intensity model
simulate	Simulation of points using random thinning
ploteffects	Plot effect of a single predictor variable in a model
roc	Receiver-operating characteristics curve
Other utilities	
as	Utility to convert PPS object to other formats
pointdistances	Pairwise distances between points in PPS
voronoi	Voronoi tessalation of the river network based on points in PPS
hasduplicates	Determine if PPS has duplicate points
removeduplicates	Remove duplicate points in PPS
convhull	Calculate convex hull of points
aggregate	Merge labelled points to a new object of PPS
idw	Inverse distance weighted interpolation on stream networks
shapewrite	Export PPS as shapefile
Visualization	
plot	Plot stream network with points
plotc	Plot colored stream network with points
ploteffects	Plot effect of covariate in a loglinear model
plotdz	Plot longitudinal profile with points
plotpoints	Plot points only
wmplot	Plot stream network with points in a webmap

A *PPS* object is created using an instance of STREAMobj and a set of coordinates of points, line features (e.g. fault traces) that intersect the stream network, or a model that randomly generates points (Figure 2). Supported models are the binomial and the homogeneous Poisson point process that randomly distribute points on the network given a specified total number of points and intensity (average number of points per unit length), respectively. For example, the pattern in Figure 1b was generated by a Poisson process with an intensity of $5\text{x}10^{-4}$ m^{-1}. Once initiated, an object of PPS can access numerous functions (or methods) which are summarized in Table 1. The functions are broadly categorized into tools for explorative analysis, inference and simulation, and visualization. In addition, there are a number of conversion tools and other utilities such as interpolation tools.

Explorative analysis of point patterns often begins with kernel density estimates to highlight spatially varying densities of points. While kernel density estimates are straightforward in 1D, 2D or higher dimensions, they are not directly applicable to networks. Conventional 2D kernel density estimators applied to points on river networks may easily overestimate densities along adjacent rivers albeit the rivers may be disconnected. Applying 1D kernel density estimators to networks, however, is also fallacious because it fails to conserve mass where networks branch (McSwiggan et al., 2017; Okabe and Sugihara, 2012). The function *density* adopts the approach of McSwiggan et al. (2017) who implement Gaussian kernel density estimation on networks using an approach that perceives Gaussian kernels as heat kernels and the variable densities along the network as Brownian diffusion (McSwiggan et al., 2017).

Clustering is a technique that groups similar objects to classes. In spatial point pattern analysis this technique is used to detect spatial clusters of points, and to merge them eventually to a set of new points. The function *cluster* uses hierarchical clustering based on the shortest-path distances of all points (Okabe and Sugihara, 2012). The resulting spatial clusters can subsequently be merged using the function *aggregate*, which computes cluster centers by finding the network node that minimizes the sum of squared shortest distances from each point in the cluster.

An important question in the analysis of point patterns is whether the intensity of points depends on spatial covariates. Parametric models describing this dependence have a long tradition in point pattern analysis. These models require that the dependence structure of the model is known. Yet, often we do not know the form of the model, or the form is too complicated to be fitted by a parametric model. Thus, nonparametric estimation provides an important exploratory approach, since it determines the model structure from the data. While nonparametric models do not completely lack parameters, they model the relationship between variables with fewer assumptions, and are thus particularly suitable for explorative analysis (Baddeley et al., 2012). We implemented this nonparametric technique in PPS with the function *rhohat*, which also calculates confidence intervals using bootstrapping.

Nonparametric analysis of covariate dependence makes no assumptions about the shape of the functional relationship between point density and an explanatory variable. However, if the type of relationship is known or hypothesized, then parametric techniques are a more powerful way to analyze the data (Baddeley et al., 2015). The most common model in point pattern analysis is the inhomogeneous Poisson point process model with an intensity which is a loglinear function of the covariates (Baddeley et al., 2015)

$$\lambda(u) = e^{B(u)+\boldsymbol{\theta}^{\mathrm{T}}\boldsymbol{Z}(u)} \quad (1)$$

where λ is the intensity of points at locations u, B is a known baseline intensity, and θ is a vector of p parameters for a vector-valued function $Z(u) = [Z_1(u) \dots Z_p(u)]$. Loglinear models assume that the intensity is intrinsically positive-valued and enables to model the dependence of intensity on numeric and categorical variables. The model assumes no interactions between points and thus has the advantage that parameter estimation can rely on standard techniques such as logistic regression or Poisson regression. PPS implements Poisson models using the function *fitloglinear*. The function accesses the function *fitglm*, which is part of the MATLAB Statistics and Machine Learning Toolbox and fits generalized linear least squares problems. PPS also features a Bayesian approach to analyze loglinear models. The function *bayesloglinear* interfaces with the BayesReg Toolbox (Makalic and Schmidt, 2011, 2016) which provides highly efficient and numerically stable implementations of penalized regression techniques.

PPS features tools to study first and second order effects in point processes. However, current inferential methods in PPS are based on models that assume that point patterns do not exhibit second order effects. Variable densities of points in space are assumed to relate to some factor or covariate. Models exist that can be used to explain clustering or regular patterns and include Cox, Neyman-Scott, Gibbs or Hawkes models. These models are currently not supported in PPS.

Case studies

Applying the techniques and tools outlined in the previous section, we present two case studies in which the analysis of point patterns is used to extract information about geomorphological processes that take place on or alongside rivers. In the first case study, we demonstrate how explorative analysis of knickpoints in river profiles of the Big Tujunga catchment in California can help reveal two phases of landscape rejuvenation. In the second case study, we investigate the spatial distribution of beaver dams in the Tualatin basin, Oregon, and model their geomorphometric constraints. For brevity, some of the data and methods of the case studies are summarized in Table 2. All data are open and freely available.

Table 2: Data used in the case studies.

Case study	Knickpoints in the Big Tujunga catchment	Beaver dams in the Tualatin basin
Location	California, USA, 34.2°N, 118.2°W	Oregon, USA, 45.4°N, 122.8°W
Catchment area	293 km^2	1803 km^2
DEM (spatial resolution)	SRTM-1 (30 m)	NED (10 m)
Point pattern	52 knickpoints detected by knickpointfinder	510 beaver dams from Smith (2019)
Additional data	Vector data with faults from (USGS and NMBMMR, 2019)	Stream network vector data from Nagel et al. (2017)

Knickpoints in the Big Tujunga basin

Rivers in the Big Tujunga catchment in the San Gabriel Mountains feature numerous knickpoints along their longitudinal profiles. These knickpoints are unrelated to lithological boundaries and they are found in relatively narrow elevation bands (Wobus et al., 2006), which suggests that they formed at the range front due to acceleration in slip rate of the Sierra Madre Fault Zone, and the concomitant adjustment of the stream network to the higher uplift rate (DiBiase et al., 2015). The aim of this example is to illustrate how an explorative analysis of knickpoint patterns helps in assessing a model of landscape response times to changes in tectonic uplift.

The most widely used model of fluvial incision and knickpoint migration is the stream power incision model (SPIM) (Lague, 2014), which states that the rate at which elevations z along a river change over time t is a function of uplift U, erosional efficiency K, upslope area A and local river gradient

$$\frac{\partial z(x)}{\partial t} = U(x,t)K(x,t)A(x,t)^m \left|\frac{dz}{dx}\right|^n \tag{2}$$

where x is the distance from the river outlet along the flow network, and the exponents m and n are empirical constants. Assuming that U and K do not vary in time and space, and that drainage configurations remain unchanged, the steady state channel slope is calculated with

$$\left|\frac{dz}{dx}\right| = \left(\frac{U}{K}\right)^{\frac{1}{n}} A(x)^{-\frac{m}{n}} \tag{3}$$

a relation between channel slope and area that predicts an upward concave river profile (Hack, 1957). Based on Eq. 3, Harkins et al. (2007) and Perron and Royden (2013) introduced a coordinate transformation which linearizes the power-law relation. The linearization takes the integral of the left and right term in Eq. 3 so that elevation becomes a linear function

$$z(x) = z(x_b) + \left(\frac{U}{KA_0^m}\right)^{\frac{1}{n}} \chi \tag{4}$$

where

$$\chi = \int_{x_b}^{x} \left(\frac{A_0}{A(x)}\right)^{\frac{m}{n}} dx \tag{5}$$

with A_0 (which we set to 10^6 m^2) and x_b is the location of the base level (Perron and Royden, 2013). The linear form of the SPIM (with n=1) predicts that perturbations to river elevations, for example by base level change, migrate upstream as a function of upstream area (Berlin and Anderson, 2007). χ-transformation normalizes for upstream area so that any base level change at x_b in the past, should result in knickpoints that cluster at a specific value of χ, irrespective of whether the perturbation has travelled upstream the trunk river, or any of its tributaries (Perron and Royden, 2013; Schwanghart and Scherler, 2020). χ thus serves as a metric for distances travelled by perturbations upstream in the river network (Fox et al., 2014).

In order to test the knickpoint celerity model in the Big Tujunga catchment, we derived a stream network with a minimum supporting upslope area of 0.9 km^2. Locations of knickpoints were calculated using the function knickpointfinder, an automated method of knickpoint identification based on iterative fitting of strictly concave stream profiles that is implemented in TopoToolbox and described in Stolle et al. (2019). Applying a tolerance of 20 m – which is about the maximum elevation error recorded along streams of the SRTM-1 (Schwanghart and Scherler, 2017) – yields 52 knickpoints (Figure 3A). Knickpoint height – the elevation difference between the fitted profile and a knickpoint, and a measure taken here for the prominence of each knickpoint – ranges between 22 and 216 m.

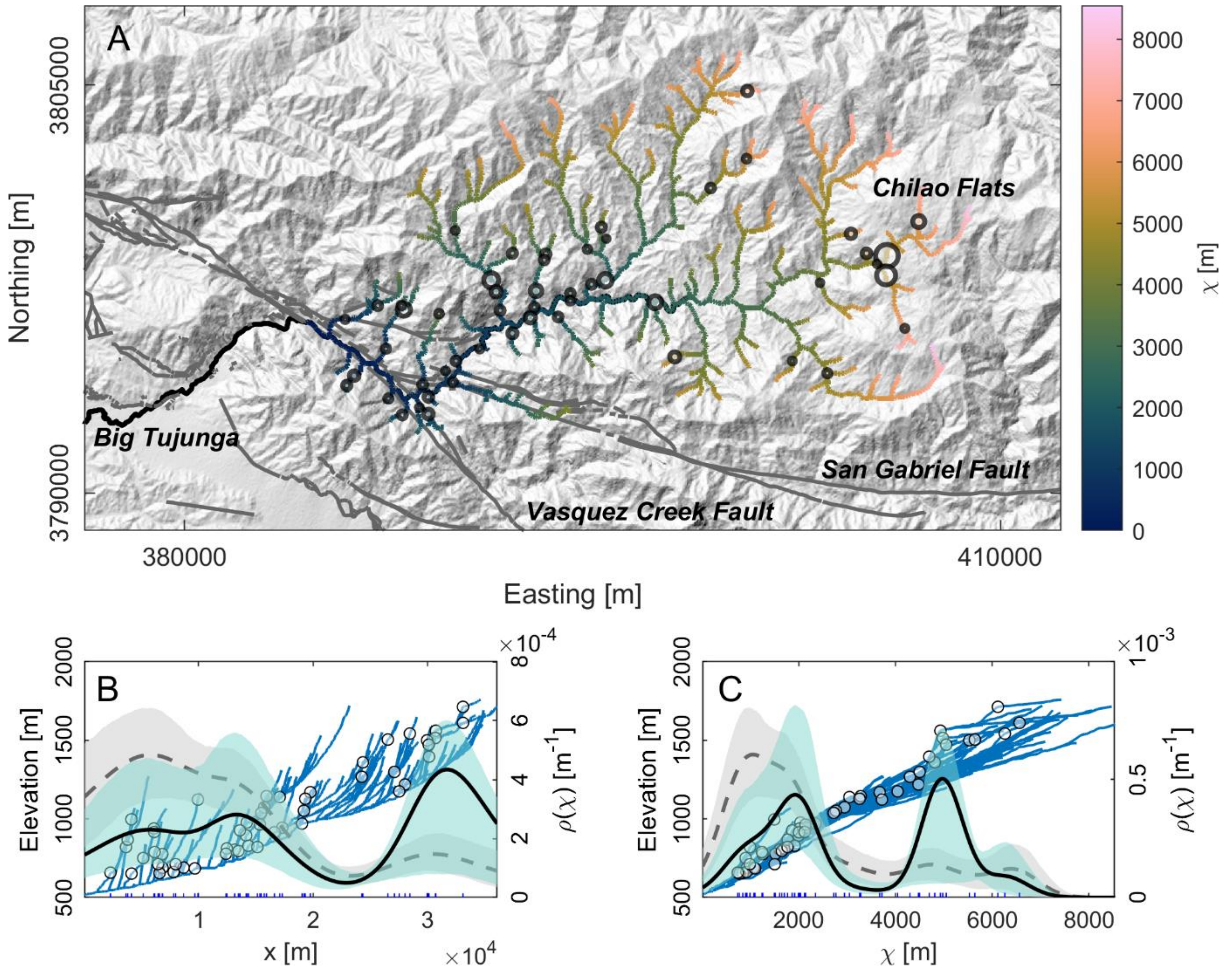

Figure 3: Knickpoint patterns in the Big Tujunga catchment. A) Hillshade map of the catchment and faults (gray lines; after Morton and Miller, 2006), knickpoints and χ-values of the river network. The size of the knickpoint symbols linearly scales with knickpoint heights, which range between 22 and 216 m. B) Distribution of knickpoints along river profiles (blue lines). Gray dashed line shows the nonparametric dependence of knickpoint locations (with gray envelopes indicating bootstrapped 95% confidence intervals) as a function of distance from the range-bounding fault. The black line shows the dependence estimate weighted by the knickpoint height. The bandwidth for both estimates is 3000 m. C) Same as B), but with the covariate being χ and bandwidth being 400 m.

The majority of knickpoints are located in the lower part of the catchment (Figure 3A), which is also reflected by the nonparametric estimate (function *rhohat*) which shows how knickpoint locations depend on the distance to the range-bounding fault (Figure 3B, dashed gray line). Weighting knickpoints by their squared heights (black line) the occurrence of few but prominent knickpoints in the upper part of the basin is accentuated. We calculated χ with an m/n ratio of 0.4 which has previously been used by Perron and Royden (2013) for the same catchment. Figure 3C is similar to B, but depicts density estimates as a function of χ. Again, a non-weighted density estimation highlights the knickpoints in the vicinity to the catchment outlet, whereas weighting them reveals two pronounced peaks at χ values around 2000 and 5000 m. However, uncertainty intervals (based on bootstrapping) of the density estimates of the second peak are high and reflect the scarcity of knickpoints in the upper part of the catchment.

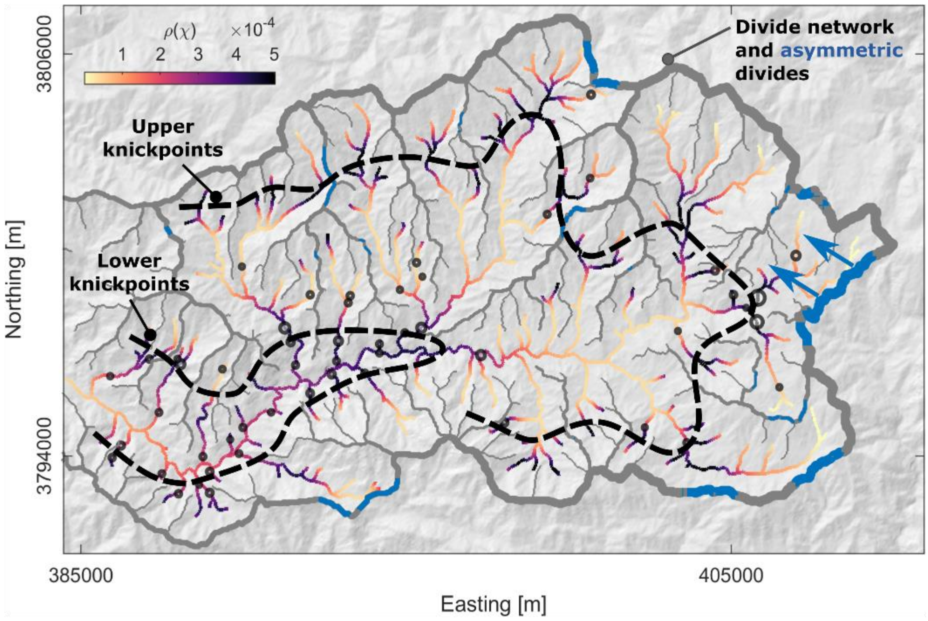

Figure 4: Actual and expected spatial patterns of knickpoints in the Big Tujunga basin. The two dashed lines are manually drawn to highlight the two generations of upstream migrating knickpoints and their expected locations. The gray lines depict the drainage divide network (Scherler and Schwanghart, 2020), with blue sections showing asymmetric divides and the inferred movement is indicated by the blue arrows.

Mapping the patterns of knickpoint density obtained from the weighted nonparametric dependence model in Figure 3C back to spatial coordinates (Figure 4) reveals the expected spatial locations of knickpoints. Clearly, as the model was obtained from actual knickpoint locations, both must be consistent to a certain degree. Notwithstanding, actual and expected knickpoint patterns show notable differences in many locations that require explanation. These differences are particularly obvious for the older wave of knickpoints that mark the transition to the Chilao Flats and that are expected to be present high up in other tributaries to the Big Tujunga as well. However, most headwater channels are devoid of knickpoints. There are several explanations for a lack of consistency between expected and actual knickpoint patterns. First, variations in bedrock erodibility manifest themselves in a series of waterfalls in the oversteppened knickzone straddling the Chilao Flats. These waterfalls have been previously found to have slowed down knickpoint retreat by at least an order of magnitude (DiBiase et al., 2015). Other tributaries may lack such resistant layers and thus knickpoints may have already left the system. Second, headwater channels may be dominated by debris-flow processes (Hergarten et al., 2016; Stock and Dietrich, 2003) which may result in faster incision and possibly smearing of knickpoints in the channels. Third, inconsistencies between expected and observed knickpoint patterns may arise from drainage reorganization. Our analysis weighted the most prominent knickpoints, yet these knickpoints may be those that have been particularly affected by divide migration. The margins of the Chilao Flats show highly asymmetric divides (Scherler and Schwanghart, 2020) (Figure 4) which suggest possibly past and ongoing drainage reorganization. Such reorganization may significantly alter drainage areas and discharge, and thus impact on knickpoint celerities which in return will result in more scattered knickpoint locations (Schwanghart and Scherler, 2020).

Beaver dams in the Tualatin basin, Oregon

Beavers are ecosystem engineers that build dams across and alongside rivers. These wood accumulations increase floodplain storage of water, sediment, organic matter and nutrients, and thus have several ecological benefits (Bouwes et al., 2016; Macfarlane et al., 2017; Wohl, 2013). As beaver dams impound water upstream, they also raise the possibility of beaver dam outburst floods. Although such outburst floods are rare, there were cases where such events greatly exceeded discharges of meteorological floods (O'Connor et al., 2013). Given both ecological benefits and outburst hazard, potential beaver dam locations should thus be known for managing river restoration and flood risk.

In this case study, our analysis focuses on topographic controls on the occurrence of beaver dams that can be derived solely from catchment-scale digital elevation data. Several properties determine the degree to which beavers colonize and sustain a population (Gurnell, 1998), and we hypothesize that beaver habitats are primarily a function of stream flow and stream gradient. Beavers require sufficient stream flow as a reliable water source. Yet, rivers should neither be too wide nor too deep to inhibit building and persistence of dams (Collen and Gibson, 2000; Gurnell, 1998; Macfarlane et al., 2017). At the same time, river gradient should be relatively low to impound sufficiently large areas. Therefore, steep and rocky rivers are generally less favored by beavers as dams in such streams are susceptible to damage during high-magnitude discharges and have low impounding efficiency (Gurnell, 1998).

To test the above hypothesis, we studied the distribution of beaver dams in the Tualatin basin, Oregon (Table 2, Figure 5A). In our analysis, we used upstream area as proxy for stream flow, which we derived from the DEM using flow accumulation. Anthropogenic features such as bridges and culverts produced some artifacts when computing the stream network from the original DEM. Thus, we used hydrographic data from Nagel et al. (2017) and preprocessed the DEM using stream burning (Reuter et al., 2009). We extracted the stream network based on an area threshold of 0.1 km^2, and smoothed the profiles using the CSR (constrained regularized smoothing) algorithm (Schwanghart and Scherler, 2017) with a smoothing factor of K = 10. The smoothed elevations are subsequently used to calculate the local stream gradient. Commonly, stream gradients derived from DEMs fluctuate strongly as they are highly sensitive to errors in the elevation data (Wobus et al., 2006). Our approach of smoothing the profiles created local gradients that mimic those obtained from a moving window approach with a kernel size of ~200 m.

Beaver dam locations were obtained from the version 2.0 of the data released by Smith (2019). The data was compiled by the U.S. Geological Survey (USGS) and comprises information on 510 beaver dams. Some recorded locations are very close to each other and likely correspond to the same beaver populations. Thus, we merged locations using the function *cluster* (Table 1). The function implements hierarchical clustering based on the shortest-path distance matrix of all points using an average linkage method. We chose a cutoff of 160 m and obtained 217 unique locations, which we used for the subsequent analysis.

The pattern of beaver dams (Figure 5A) suggests that their intensity is spatially inhomogeneous. This hypothesis can be tested using techniques such as quadrat counting (function *quadratcount*). Quadrat counting subdivides the network into roughly equal sized subnetworks and then counts the number of locations within each subnetwork. Under the assumption of complete spatial randomness, the distribution of points in each subnetwork should follow a Poisson distribution with homogeneous intensity, a hypothesis that we investigate with a χ^2-test (note that χ^2 has nothing in common with the χ-transformation in the previous case study). The χ^2-test underscores ($p<0.0001$) the visual impression that spatial locations of beaver dams in the Tualatin Basin are not completely random.

To test whether drainage area and stream gradient can be used to explain spatial variations in beaver-dam density, we fit a loglinear model with stream gradient and the decadic logarithm of upslope area as independent variables. The loglinear model has an intercept and a first-degree polynomial for gradient and second-degree polynomial for upslope area. Moreover, we add an interaction term (product of both predictors) to investigate whether the interrelationship of stream gradient and upslope area determines spatial beaver-dam densities.

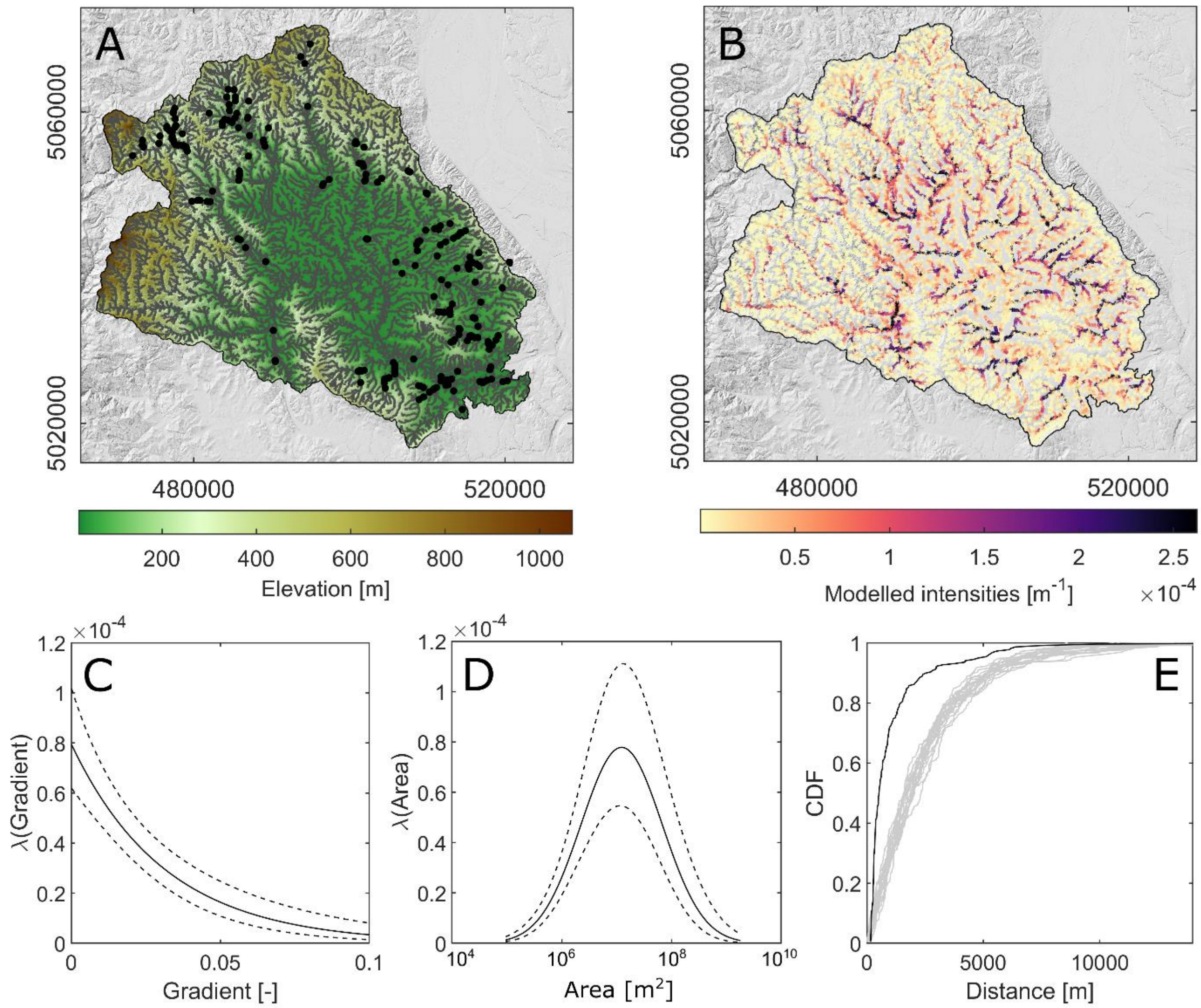

Figure 5: Modelling the locations of beaver dams in the Tualatin basin, Oregon, US. A) Hillshade map of the basin, stream network, and the locations of beaver dams (black dots). B) Modelled intensities of beaver dams using an inhomogeneous Poisson point pattern. C+D) Fitted responses to a single predictor: C) Stream gradient and D) drainage area. E) Empirical nearest-neighbor distance distribution function for actual beaver dam locations (solid black line) compared to distribution functions of 20 simulated point patterns derived from the inhomogeneous Poisson model (gray lines).

We fit the model using stepwise regression which removes parameters or terms that fail to improve the model fit measured by the Akaike-Information Criterion (AIC). Stepwise regression removes the interaction term so that the final model is

$$\hat{\lambda}(u) = e^{\beta_0+\beta_1 g(u)+\beta_2 a(u)+\beta_3 a^2(u)} \quad (6)$$

where $\hat{\lambda}$ is the estimated density of beaver dams (Figure 5B), β_0 is an offset, and β_{1-3} are the parameters for stream gradient g and the decadic logarithm of upslope area a and its quadratic form, respectively. Overall, the model is highly significant compared to a model with a pure offset (p = $7.28\text{x}10^{-82}$) and the area under the ROC (receiver-operating characteristic) curve, a measure of aggregated classification performance, is 0.85 (0.83-0.86 simulation confidence intervals). The values for the parameters, their uncertainties and individual p-values are listed in Table 3 and the fitted responses to the single variables are shown in Figure 5C and D.

Table 3: Estimated parameters of a loglinear model of beaver-dam locations in the Tualatin basin, Oregon, US.

	Estimate	SE	t-statistics	p-value
$\boldsymbol{\beta_0}$	-51.99	4.62	-11.26	2.18E-29
$\boldsymbol{\beta_1}$	-31.60	4.99	-6.33	2.48E-10
$\boldsymbol{\beta_2}$	12.97	1.36	9.55	1.35E-21
$\boldsymbol{\beta_3}$	-0.91	0.10	-9.20	3.68E-20

Although the model provides a reasonable fit to the data, it may neglect other potential factors. Previous studies found that stream depth, sandbar width, and anabranching (secondary rivers, sloughs) as well as access to forage are important controls on the spatial distribution of beaver dams (e.g. Scrafford et al., 2018). Our data and the representation of the flow network by D8 flow directions do not permit us to represent these factors. In addition, beaver dams entail hydrologic (creating wetlands), hydraulic (slow down runoff), geomorphic (sediment trapping), and ecological feedbacks (subirrigation of downstream valley bottoms that promotes establishment and expansion of riparian vegetation); all of which tend to increase stream complexity and channel-floodplain connectivity (Macfarlane et al., 2017). These feedbacks may lead to spatial clustering, as beaver-engineered river reaches may increase local beaver populations. Our model does not capture such clustering effects. However, to test whether the data exhibits such spatial clustering after accounting for the first-order effects of stream gradient and discharge, we simulated 20 realizations of beaver dam locations using our model (function *simulate*), each time measuring the cumulative distribution of nearest neighbor distances (the G-statistics as measured by the function *gfun* (Baddeley et al., 2015)). Figure 5E shows that the actual distribution of beaver dams exhibits a much stronger clustering compared to the simulated points although we declustered the original data. Whether this clustering may evolve from individual beaver populations or positive feedbacks exerted by beavers on their habitats remains shrouded. However, modelling such interactions may improve with more advanced point pattern models, whose treatment is beyond the scope of this study and which are currently not implemented in PPS.

Discussion

The two studies that we presented showcase the new TopoToolbox extension PPS, which supports the analysis of point patterns on stream networks. The studies have in common that different geomorphic phenomena can be conceptualized as point processes that occur on or alongside stream networks. Knickpoints in bedrock rivers, for example, migrate upstream along the river network, but with no apparent link between adjacent rivers. This strict constraint could be relaxed when analyzing beaver populations because beavers may shortcut distances between adjacent rivers when expanding into new territory. Our analysis did not take the potential movement of beavers between streams into account, which may in particular affect second-order patterns of beaver dams. To this end, investigating such effects would require distance metrics between points that combine distances along and aside stream networks.

Our case study on the spatial distribution of knickpoint relied on weighting knickpoints by their height. Yet, we didn't include such attributes in the analysis of beaver dams, although these biogeomorphic features commonly have highly variable sizes (Turowski et al., 2013), which could be used to weight observations in the models. While such attribute data was not available in this study, we note that it may be useful to record this data when recording point pattern data in the field. Moreover, additional attribute data could be used in the analysis of marked point patterns, a suite of methods to explore and model point patterns with attribute data. However, such techniques are currently not yet available in PPS.

PPS relies on the geographic representation of geomorphic objects or features as points, and streams as lines or network of lines. It follows that the studied phenomena must be conceptualized as points, although they may often have volumes associated with them and they may have vaguely defined limits or be overlapping (Evans, 2012; Goodchild, 2011; Smith, 2011). As common in GIS analysis, such a representation embodies spatial scale to some degree. For point pattern analysis, it is crucial to remember that spacing between points may be observed if points actually represent areal nonoverlapping features. Moreover, as points are constrained to lie on nodes of the stream network, which are derived from the underlying DEM, the representation of network events is tightly linked to the spatial resolution of the DEM. This also entails that the density of points should not be too high, as it may cause points to share the same locations, a situation usually not foreseen in point pattern analysis. In addition, the distance between two vertices is a lower bound of the true distance, if we assume that all line vertices are located on the central line of the river (Goodchild, 2011). In TopoToolbox and thus also PPS, the geometry of stream networks is determined by the Moore neighborhood (8-connectivity) of the D8 flow direction algorithm. This means that cell centers are rarely on the centerline of the actual stream and that river lengths can be both over- and underestimated. Underestimation typically occurs for low resolution grids, while overestimation occurs for high-resolution DEMs and relatively straight rivers. Relative errors in river length have been estimated to range from 5-7% for distances calculated on raster data structures, and up to >30% for very coarse resolution DEMs (Paz et al., 2008). In point pattern analysis, these errors will affect estimates of point intensity and interpoint distances. Hence, models developed with a particular DEM, cannot be easily transferred to other DEMs without analyzing how these DEMs affect distance calculations.

Only few functions in PPS account for the directedness of stream networks. For example, the function pointdistances enables to calculate nearest neighbor distances in upstream and downstream directions. Most functions, however, treat the network as undirected and thus neglect that many processes on stream networks have a natural direction. Sediment and nutrient transport, for example, will follow the downstream flow of water, while mobile knickpoints commonly migrate upstream. Although techniques of geostatistical interpolation that account for the directional dependence of dispersal in river networks exist (Garreta et al., 2010), in point pattern analysis, these approaches are rare and a relatively new field of research (Rasmussen and Christensen, 2019).

We envision numerous other potential applications of PPS. Beyond the case studies shown, potential applications include the analysis of sediment tracers, the locations of outsized boulders, wood jams, or landslide dams. In addition, PPS may be applied in ecology for modelling of aquatic species based on sightings, for example. Finally, once point pattern models have been trained, they can be adopted in simulation tools such as the TopoToolbox Landscape Evolution Model (TTLEM) (Campforts et al., 2017) to study the stochastic forcing of landslides on riverscapes in long-term landscape development.

Conclusions

PPS is a new numeric class in TopoToolbox for the analysis of point patterns on stream networks. In two case studies, we analyzed geomorphic phenomena whose locations are constrained to river networks. Combining explorative analysis of the locations of knickpoints with χ-analysis in the Big Tujunga catchment, PPS allowed us to identify two distinct generations of knickpoints. In our analysis of beaver dams, we have shown that the inhomogeneous Poisson process models implemented in PPS helps to infer different geomorphological factors on beaver habitats.

PPS focuses on exploratory data analysis and fitting of inhomogeneous Poisson point processes, which both allow studying covariates that control the spatial density of points. In addition, PPS features numerous tools for simulation and visualization. Incorporation into TopoToolbox enables ease of access to these new functionalities from within one computational environment. Besides the presented case studies, we anticipate other applications of PPS for studying processes in fluvial geomorphology and landscape evolution, but it also the distribution of aquatic and riparian species or other phenomena that are constrained to occur on or alongside rivers.

Acknowledgments

We thank Cassandra D. Smith and the USGS for access to the data on beaver dam locations. Opentopography was used to download some of the DEMs used in this study. Some figures were made using Scientific Colormaps (Crameri, 2018).

References

Ang QW, Baddeley A, Nair G. 2012. Geometrically Corrected Second Order Analysis of Events on a Linear Network, with Applications to Ecology and Criminology. Scandinavian Journal of Statistics **39** : 591–617. DOI: 10.1111/j.1467-9469.2011.00752.x

Baddeley A, Chang Y-M, Song Y, Turner R. 2012. Nonparametric estimation of the dependence of a spatial point process on spatial covariates. Statistics and Its Interface **5** : 221–236. DOI: 10.4310/SII.2012.v5.n2.a7

Baddeley A, Rubak E, Turner R. 2015. Spatial Point Patterns: Methodology and Applications with R . Apple Academic Press Inc.: Boca Raton ; London ; New York

Berlin MM, Anderson RS. 2007. Modeling of knickpoint retreat on the Roan Plateau, western Colorado. Journal of Geophysical Research: Earth Surface **112** DOI: 10.1029/2006JF000553 [online] Available from: https://agupubs.onlinelibrary.wiley.com/doi/abs/10.1029/2006JF000553 (Accessed 17 July 2018)

Bishop MA. 2007a. Point pattern analysis of eruption points for the Mount Gambier volcanic sub-province: a quantitative geographical approach to the understanding of volcano distribution. Area **39** : 230–241. DOI: 10.1111/j.1475-4762.2007.00729.x

Bishop MA. 2007b. Point pattern analysis of north polar crescentic dunes, Mars: A geography of dune self-organization. Icarus **191** : 151–157. DOI: 10.1016/j.icarus.2007.04.027

Bouwes N, Weber N, Jordan CE, Saunders WC, Tattam IA, Volk C, Wheaton JM, Pollock MM. 2016. Ecosystem experiment reveals benefits of natural and simulated beaver dams to a threatened population of steelhead (Oncorhynchus mykiss). Scientific Reports **6** : 1–12. DOI: 10.1038/srep28581

Braun J, Willett SD. 2013. A very efficient O(n), implicit and parallel method to solve the stream power equation governing fluvial incision and landscape evolution. Geomorphology **180–181** : 170–179. DOI: 10.1016/j.geomorph.2012.10.008

Campforts B, Schwanghart W, Govers G. 2017. Accurate simulation of transient landscape evolution by eliminating numerical diffusion: the TTLEM 1.0 model. Earth Surface Dynamics **5** : 47–66. DOI: 10.5194/esurf-5-47-2017

Clark CD, Ely JC, Spagnolo M, Hahn U, Hughes ALC, Stokes CR. 2018. Spatial organization of drumlins. Earth Surface Processes and Landforms **43** : 499–513. DOI: 10.1002/esp.4192

Collen P, Gibson RJ. 2000. The general ecology of beavers (Castor spp.), as related to their influence on stream ecosystems and riparian habitats, and the subsequent effects on fish – a review. Reviews in Fish Biology and Fisheries **10** : 439–461. DOI: 10.1023/A:1012262217012

Crameri F. 2018. Geodynamic diagnostics, scientific visualisation and StagLab 3.0. Geoscientific Model Development **11** : 2541–2562. DOI: https://doi.org/10.5194/gmd-11-2541-2018

Cressie N, Frey J, Harch B, Smith M. 2006. Spatial prediction on a river network. Journal of Agricultural, Biological, and Environmental Statistics **11** : 127. DOI: 10.1198/108571106X110649

DiBiase RA, Whipple KX, Lamb MP, Heimsath AM. 2015. The role of waterfalls and knickzones in controlling the style and pace of landscape adjustment in the western San Gabriel Mountains, California. Geological Society of America Bulletin **127** : 539–559.

Evans IS. 2012. Geomorphometry and landform mapping: What is a landform? Geomorphology **137** : 94–106. DOI: 10.1016/j.geomorph.2010.09.029

Fan X et al. 2020. The formation and impact of landslide dams – State of the art. Earth-Science Reviews **203** : 103116. DOI: 10.1016/j.earscirev.2020.103116

Foltête JC, Berthier K, Cosson JF. 2008. Cost distance defined by a topological function of landscape. Ecological Modelling **210** : 104–114. DOI: 10.1016/j.ecolmodel.2007.07.014

Fonstad MA, Marcus WA. 2003. Self-organized criticality in riverbank systems. Annals of the Association of American Geographers **93** : 281–296.

Fox M, Goren L, May DA, Willett SD. 2014. Inversion of fluvial channels for paleorock uplift rates in Taiwan. Journal of Geophysical Research: Earth Surface **119** : 1853–1875. DOI: 10.1002/2014JF003196

Gailleton B, Mudd SM, Clubb FJ, Peifer D, Hurst MD. 2019. A segmentation approach for the reproducible extraction and quantification of knickpoints from river long profiles. Earth Surface Dynamics **7** : 211–230. DOI: https://doi.org/10.5194/esurf-7-211-2019

Ganio LM, Torgersen CE, Gresswell RE. 2005. A geostatistical approach for describing spatial pattern in stream networks. Frontiers in Ecology and the Environment **3** : 138–144. DOI: 10.1890/1540-9295(2005)003[0138:AGAFDS]2.0.CO;2

Garreta V, Monestiez P, Ver Hoef JM. 2010. Spatial modelling and prediction on river networks: up model, down model or hybrid? Environmetrics **21** : 439–456. DOI: 10.1002/env.995

Golly A, Turowski JM, Badoux A, Hovius N. 2019. Testing models of step formation against observations of channel steps in a steep mountain stream. Earth Surface Processes and Landforms **44** : 1390–1406. DOI: 10.1002/esp.4582

Goodchild MF. 2011. Scale in GIS: An overview. Geomorphology **130** : 5–9. DOI: 10.1016/j.geomorph.2010.10.004

Gurnell AM. 1998. The hydrogeomorphological effects of beaver dam-building activity. Progress in Physical Geography: Earth and Environment **22** : 167–189. DOI: 10.1177/030913339802200202

Hack JT. 1957. Studies of longitudinal stream profiles in Virginia and Maryland. USGS Professional Paper **295** : 45–97.

Harkins N, Kirby E, Heimsath A, Robinson R, Reiser U. 2007. Transient fluvial incision in the headwater of the Yellow River, northeastern Tibet, China. Journal of Geophysical Research **112** : F03S04-F03S04. DOI: 10.1029/2006JF000570

Heckmann T, Schwanghart W, Phillips JD. 2015. Graph theory—Recent developments of its application in geomorphology. Geomorphology **243** : 130–146. DOI: 10.1016/j.geomorph.2014.12.024

Hergarten S, Neugebauer HJ. 2001. Self-Organized Critical Drainage Networks. Physical Review Letters **86** : 2689–2692. DOI: 10.1103/PhysRevLett.86.2689

Hergarten S, Robl J, Stüwe K. 2016. Tectonic geomorphology at small catchment sizes – extensions of the stream-power approach and the χ method. Earth Surface Dynamics **4** : 1–9. DOI: 10.5194/esurf-4-1-2016

Kandakji T, Gill TE, Lee JA. 2020. Identifying and characterizing dust point sources in the southwestern United States using remote sensing and GIS. Geomorphology **353** : 107019. DOI: 10.1016/j.geomorph.2019.107019

Knighton D. 1998. Fluvial Forms and Processes: A New Perspective . 2 Rev ed. Taylor & Francis Ltd: London, New York

Korup O. 2006. Rock-slope failure and the river long profile. Geology **34** : 45–48. DOI: 10.1130/G21959.1

Kraft CE, Warren DR, Keeton WS. 2011. Identifying the spatial pattern of wood distribution in northeastern North American streams. Geomorphology **135** : 1–7. DOI: 10.1016/j.geomorph.2011.07.019

Lague D. 2014. The stream power river incision model: evidence, theory and beyond. Earth Surface Processes and Landforms **39** : 38–61. DOI: 10.1002/esp.3462

Liang C, Jaksa MB, Kuo YL, Ostendorf B. 2015. Identifying areas susceptible to high risk of riverbank collapse along the Lower River Murray. Computers and Geotechnics **69** : 236–246. DOI: 10.1016/j.compgeo.2015.05.019

Lombardo L, Bakka H, Tanyas H, Westen C van, Mai PM, Huser R. 2019. Geostatistical Modeling to Capture Seismic-Shaking Patterns From Earthquake-Induced Landslides. Journal of Geophysical Research: Earth Surface **124** : 1958–1980. DOI: 10.1029/2019JF005056

Lombardo L, Opitz T, Huser R. 2018. Point process-based modeling of multiple debris flow landslides using INLA: an application to the 2009 Messina disaster. Stochastic Environmental Research and Risk Assessment **32** : 2179–2198. DOI: 10.1007/s00477-018-1518-0

Macfarlane WW, Wheaton JM, Bouwes N, Jensen ML, Gilbert JT, Hough-Snee N, Shivik JA. 2017. Modeling the capacity of riverscapes to support beaver dams. Geomorphology **277** : 72–99. DOI: 10.1016/j.geomorph.2015.11.019

Makalic E, Schmidt DF. 2011. A Simple Bayesian Algorithm for Feature Ranking in High Dimensional Regression Problems. Berlin, Heidelberg. 223–230 pp.

Makalic E, Schmidt DF. 2016. High-Dimensional Bayesian Regularised Regression with the BayesReg Package [online] Available from: https://arxiv.org/abs/1611.06649v3 (Accessed 30 January 2020)

McSwiggan G, Baddeley A, Nair G. 2017. Kernel Density Estimation on a Linear Network. Scandinavian Journal of Statistics **44** : 324–345. DOI: 10.1111/sjos.12255

Nagel D, Wollrab S, Parkes-Payne E, Peterson E, Isaak D, Ver Hoef J. 2017. National Stream Internet hydrography datasets for spatial-stream-network (SSN) analysis

O'Connor JE, Clague JJ, Walder JS, Manville V, Beebee RA. 2013. Outburst Floods. In Treatise on Geomorphology , . Elsevier; 475–510. [online] Available from: https://linkinghub.elsevier.com/retrieve/pii/B9780123747396002517 (Accessed 30 September 2019)

Oeppen BJ, Ongley ED. 1975. Spatial Point Processes Applied to the Distribution of River Junctions. Geographical Analysis **7** : 153–171. DOI: 10.1111/j.1538-4632.1975.tb01032.x

Okabe A, Okunuki K-I, SANET Team. 2018. SANET. A spatial analysis along networks (Ver. 4.1) . Tokyo, Japan

Okabe A, Satoh T, Sugihara K. 2009. A kernel density estimation method for networks, its computational method and a GIS-based tool. International Journal of Geographical Information Science **23** : 7–32. DOI: 10.1080/13658810802475491

Okabe A, Sugihara K. 2012. Spatial analysis along networks: statistical and computational methods . John Wiley & Sons: Chicheser

Paz AR da, Collischonn W, Risso A, Mendes CAB. 2008. Errors in river lengths derived from raster digital elevation models. Computers & Geosciences **34** : 1584–1596. DOI: 10.1016/j.cageo.2007.10.009

Perron JT, Royden L. 2013. An integral approach to bedrock river profile analysis. Earth Surface Processes and Landforms **38** : 570–576. DOI: 10.1002/esp.3302

Phillips JD, Lutz JD. 2008. Profile convexities in bedrock and alluvial streams. Geomorphology **102** : 554–566. DOI: 10.1016/j.geomorph.2008.05.042

Rakshit S, Nair G, Baddeley A. 2017. Second-order analysis of point patterns on a network using any distance metric. Spatial Statistics **22** : 129–154. DOI: 10.1016/j.spasta.2017.10.002

Rasmussen JG, Christensen HS. 2019. Point processes on directed linear network. arXiv:1812.09071 [math, stat] [online] Available from: http://arxiv.org/abs/1812.09071 (Accessed 11 March 2020)

Reuter HI, Hengl T, Gessler P, Soille P. 2009. Preparation of DEMs for geomorphometric analysis. In Geomorphometry. Concepts, Software, Applications , Hengl T and Reuter HI (eds). Elsevier; 87–120.

Scherler D, Schwanghart W. 2020. Drainage divide networks – Part 1: Identification and ordering in digital elevation models. Earth Surface Dynamics **8** : 245–259. DOI: https://doi.org/10.5194/esurf-8-245-2020

Schwanghart W, Kuhn NJ. 2010. TopoToolbox: A set of Matlab functions for topographic analysis. Environmental Modelling & Software **25** : 770–781. DOI: 10.1016/j.envsoft.2009.12.002

Schwanghart W, Scherler D. 2014. TopoToolbox 2 – MATLAB-based software for topographic analysis and modeling in Earth surface sciences. Earth Surface Dynamics **2** : 1–7. DOI: 10.5194/esurf-2-1-2014

Schwanghart W, Scherler D. 2017. Bumps in river profiles: uncertainty assessment and smoothing using quantile regression techniques. Earth Surface Dynamics **5** : 821–839. DOI: 10.5194/esurf-5-821-2017

Schwanghart W, Scherler D. 2020. Divide mobility controls knickpoint migration on the Roan Plateau (Colorado, USA). Geology DOI: 10.1130/G47054.1 [online] Available from: https://pubs.geoscienceworld.org/geology/article/doi/10.1130/G47054.1/583705/Divide-mobility-controls-knickpoint-migration-on (Accessed 27 April 2020)

Scott DN, Wohl E, Yochum SE. 2019. Wood Jam Dynamics Database and Assessment Model (WooDDAM): A framework to measure and understand wood jam characteristics and dynamics. River Research and Applications **35** : 1466–1477. DOI: 10.1002/rra.3481

Scrafford MA, Tyers DB, Patten DT, Sowell BF. 2018. Beaver Habitat Selection for 24 Yr Since Reintroduction North of Yellowstone National Park. Rangeland Ecology & Management **71** : 266–273. DOI: 10.1016/j.rama.2017.12.001

Skoien JO, Merz R, Blöschl G. 2006. Top-kriging -- geostatistics on stream networks. Hydrology and Earth System Sciences **10** : 277–287.

Smith CD. 2019. Beaver dam locations and beaver activity in the Tualatin Basin, Oregon, between 2011 and 2019 (ver. 2.0, November 2019). U.S. Geological Survey data release DOI: 10.5066/F7PZ57QP

Smith MJ. 2011. Chapter Eight - Digital Mapping: Visualisation, Interpretation and Quantification of Landforms. In Developments in Earth Surface Processes , Smith MJ, Paron P, and Griffiths JS (eds).

Elsevier; 225–251. [online] Available from: http://www.sciencedirect.com/science/article/pii/B9780444534460000082 (Accessed 31 March 2020)

Sochan A, Łagodowski ZA, Nieznaj E, Beczek M, Ryzak M, Mazur R, Bobrowski A, Bieganowski A. 2019. Splash of Solid Particles as a Stochastic Point Process. Journal of Geophysical Research: Earth Surface **124** : 2475–2490. DOI: 10.1029/2018JF004993

Stock J, Dietrich WE. 2003. Valley incision by debris flows: Evidence of a topographic signature. Water Resources Research **39** DOI: 10.1029/2001WR001057 [online] Available from: http://onlinelibrary.wiley.com/doi/10.1029/2001WR001057/abstract (Accessed 8 September 2015)

Stolle A et al. 2019. Protracted river response to medieval earthquakes. Earth Surface Processes and Landforms **44** : 331–341. DOI: 10.1002/esp.4517

Tacconi Stefanelli C, Catani F, Casagli N. 2015. Geomorphological investigations on landslide dams. Geoenvironmental Disasters **2** DOI: 10.1186/s40677-015-0030-9 [online] Available from: http://www.geoenvironmental-disasters.com/content/2/1/21 (Accessed 13 January 2020)

Tarboton DG, Bras RL, Rodriguez-Iturbe I. 1989. Scaling and elevation in river networks. Water Resources Research **25** : 2037–2051. DOI: 10.1029/WR025i009p02037

Turowski JM, Badoux A, Bunte K, Rickli C, Federspiel N, Jochner M. 2013. The mass distribution of coarse particulate organic matter exported from an Alpine headwater stream. Earth Surface Dynamics **1** : 1–11. DOI: https://doi.org/10.5194/esurf-1-1-2013

USGS, NMBMMR. 2019. Quaternary fault and fold database for the United States [online] Available from: https://www.usgs.gov/natural-hazards/earthquake-hazards/faults (Accessed 1 August 2019)

Ver Hoef JM, Peterson E, Theobald D. 2006. Spatial statistical models that use flow and stream distance. Environmental and Ecological Statistics **13** : 449–464.

Wobus C, Whipple KX, Kirby E, Snyder N, Johnson J, Spyropolou K, Crosby B, Sheehan D. 2006. Tectonics from topography: procedures, promise, and pitfalls. GSA Special Papers **398** : 55–74. DOI: 10.1130/2006.2398(04)

Wohl E. 2013. Floodplains and wood. Earth-Science Reviews **123** : 194–212. DOI: 10.1016/j.earscirev.2013.04.009